High precision measurements of ^{26}Na β^- decay

G. F. Grinyer,[1,*] C. E. Svensson,[1] C. Andreoiu,[1] A. N. Andreyev,[2] R. A. E. Austin,[3,†] G. C. Ball,[2] R. S. Chakrawarthy,[2] P. Finlay,[1] P. E. Garrett,[1,2] G. Hackman,[2] J. C. Hardy,[4] B. Hyland,[1] V. E. Iacob,[4] K. A. Koopmans,[3] W. D. Kulp,[5] J. R. Leslie,[6] J. A. Macdonald,[2] A. C. Morton,[2] W. E. Ormand,[7] C. J. Osborne,[2] C. J. Pearson,[2] A. A. Phillips,[1] F. Sarazin,[2,‡] M. A. Schumaker,[1] H. C. Scraggs,[2,§] J. Schwarzenberg,[8] M. B. Smith,[2] J. J. Valiente-Dobón,[1] J. C. Waddington,[3] J. L. Wood,[5] and E. F. Zganjar[9]

[1]*Department of Physics, University of Guelph, Guelph, Ontario, N1G 2W1 Canada*
[2]*TRIUMF, 4004 Wesbrook Mall, Vancouver, British Columbia, V6T 2A3 Canada*
[3]*Department of Physics and Astronomy, McMaster University, Hamilton, Ontario, L8S 4K1 Canada*
[4]*Cyclotron Institute, Texas A&M University, College Station, Texas 77843*
[5]*School of Physics, Georgia Institute of Technology, Atlanta, Georgia 30332-0430*
[6]*Department of Physics, Queen's University, Kingston, Ontario, K7L 3N6 Canada*
[7]*Lawrence Livermore National Laboratory, Livermore, California 94551*
[8]*Department of Nuclear Physics, University of Vienna, Waehringerstrasse 17, Vienna, A-1090 Austria*
[9]*Department of Physics and Astronomy, Louisiana State University, Baton Rouge, Louisiana 70803-4001*

(Received 22 November 2004; published 21 April 2005)

High-precision measurements of the half-life and β-branching ratios for the β^- decay of ^{26}Na to ^{26}Mg have been measured in β-counting and γ-decay experiments, respectively. A 4π proportional counter and fast tape transport system were employed for the half-life measurement, whereas the γ rays emitted by the daughter nucleus ^{26}Mg were detected with the 8π γ-ray spectrometer, both located at TRIUMF's isotope separator and accelerator radioactive beam facility. The half-life of ^{26}Na was determined to be $T_{1/2} = 1.07128 \pm 0.00013 \pm 0.00021$ s, where the first error is statistical and the second systematic. The $\log ft$ values derived from these experiments are compared with theoretical values from a full *sd*-shell model calculation.

DOI: 10.1103/PhysRevC.71.044309 PACS number(s): 21.10.Tg, 23.20.Lv, 27.30.+t

I. INTRODUCTION

A broad experimental program in superallowed Fermi β-decay studies has been initiated at TRIUMF's Isotope Separator and Accelerator (ISAC) facility [1]. The goal of these studies is to precisely determine $\log ft$ values for several of the superallowed decays that provide a demanding test of the standard model description of weak interactions [2]. As part of this program, techniques are being developed for high-precision lifetime and β-branching-ratio measurements with the recently installed 8π γ-ray spectrometer [3]. As a test case of the methodology, a series of experiments have been performed with radioactive beams of ^{26}Na. Although not a superallowed decay, ^{26}Na β^- decay provides an attractive case to study because beams of ^{26}Na are readily available from the existing ISAC surface ionization source, the daughter ^{26}Mg is stable, and 100% of β decays are followed by γ-ray emission. Under these conditions, precision measurements of the β-branching ratios from the decay ^{26}Na can be obtained from the γ-ray activity. These results provide a stringent test of the shell-model calculations over a wide range of decay energies and transition intensities.

In the first experiment, radioactive beams of $\sim 10^5$ ions per second of ^{26}Na were produced by bombarding an 18.9-g/cm^2 silicon-carbide target with up to 30 μA of 500-MeV protons from the TRIUMF main cyclotron. The second experiment utilized beams of ^{26}Na produced from a 21.8-g/cm^2 tantulum target with up to 40 μA of primary beam current. Following proton bombardment, reaction products enter a coupled surface ionization source [4] that efficiently ionizes alkali metal species such as Na. Mass separated beam ($A = 26$ in this work) can then be delivered to a number of experimental facilities in the ISAC hall.

The results presented in this article are divided into three main categories. In Sec. II we present the measurement of the half-life of ^{26}Na from a β-counting experiment that employed a 4π continuous gas flow proportional counter and fast tape transport system [5]. In Sec. III, the β-branching ratios deduced from the γ activity and measured with the 8π γ-ray spectrometer are discussed. Combining the results of Secs. II and III with the known ground-state Q value (9352 $\pm$ 6 keV [6,7]) and excited-state-level energies, the $\log ft$ values for this decay are then calculated and compared in Sec. IV of this work to a theoretical description obtained from a full *sd*-shell-model calculation.

*Electronic address: ggrinyer@physics.uoguelph.ca
†Present Address: Department of Astronomy and Physics, St. Mary's University, Halifax, Nova Scotia B3H 3C3, Canada.
‡Present Address: Department of Physics, Colorado School of Mines, Golden, Colorado 80401, USA.
§Present Address: Department of Physics, University of Liverpool, Liverpool L69 7ZE, U.K.

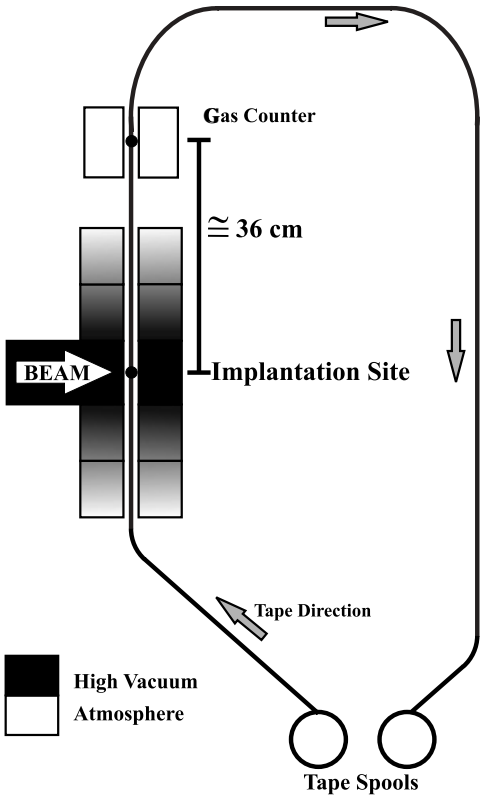

FIG. 1. Schematic of the 4π continuous gas flow proportional counter and fast tape transport system used in the β-counting experiment.

II. HALF-LIFE DETERMINATION

A. Experiment

The half-life of ^{26}Na was measured using a 4π continuous gas flow proportional counter and fast tape transport system. This experimental facility has been described in detail in previous articles [5,8,9]. A schematic of the apparatus is shown in Fig. 1. Radioactive beams of ^{26}Na for this experiment were produced from the ISAC surface ionization source coupled to a SiC target. The mass separator was operated in the high transmission efficiency mode with mass resolution $\Delta m/m \approx 1/1000$. Although able to distinguish between neighboring A values, this mode does leave the possibility of isobaric contamination. It was found in this experiment that a small contamination ($\approx$0.3%) of ^{26m}Al ($T_{1/2} = 6.3449 \pm 0.0019$ s [10]) was present in the beam.

Following mass separation, the beam was delivered to the β-counting station and implanted into a section of aluminized mylar tape (denoted by a closed circle in Fig. 1) for 0.5 s under vacuum. The beam was then turned off by deflecting it at the ion source. Following implantation, the sample was rapidly moved out of vacuum and into the 4π proportional counter, where β particles from the decay of the sample were recorded for 25–50 half-lives (altered on a run-by-run basis). The distance between the center of the detector and the beam implantation site was approximately 36 cm, as indicated in Fig. 1. With a tape speed of 2 m/s used in this experiment, the time taken for the tape to move from the implantation site to the proportional counter was approximately 0.18 s. Following the counting of the first sample, the beam would turn on for another 0.5 s, implanting a second sample onto a second region of the tape and the cycle would repeat. The collection of a single sample will be referred to as a "cycle," whereas the collection of several cycles ($\sim$200) under the same experimental conditions constituted an entire "run." The total data set collected was composed of 24 runs.

Two multichannel scalars (MCSs) were used to independently bin the data into 250 channels of adjustable bin time lengths. Two nonretriggerable gate generators were used to send well-defined pulse widths of either $\tau_1 \approx 3$ μs or $\tau_2 \approx 4$ μs to each of the MCSs. These pulse widths established a fixed dead time per event that were much longer than any of the series dead times in the system and were measured to be $\tau_1 = 3.024 \pm 0.012$ μs and $\tau_2 = 4.036 \pm 0.012$ μs by the source-pulser method [11]. One dead time was applied to each of the MCSs, and they were interchanged approximately halfway through the experiment to test for consistency between the two scalars. Binned decay data obtained from each cycle were stored separately (i.e., *not* summed). Between runs, parameters such as bin times, dead times, and detector operating voltages were modified to explore potential systematic effects.

B. Data preselection

Data were accepted providing they met the following two selection criteria. A window was set (unique to each run) that rejected all cycles if the total number of counts fell above or below the maximum and minimum values prescribed. Anomalous cycles such as those where the primary proton beam was turned off were removed by this criterion. The data were then dead-time corrected following the procedures of Ref. [9] and fit cycle by cycle, with the final selection criterion being a rejection of all cycles whose fit yielded a reduced χ^2 in excess of 1.4. The probability of exceeding a χ^2/ν of 1.4 with 245 degrees of freedom (250 bins, 5 fit parameters) is $\approx$0.002%. This rejection criterion was designed to remove any cycles in which an electrical discharge in the gas counter produced noise in the spectrum. This final criterion removed no cycles from the data set. That is $\chi^2/\nu <$ 1.4 for every individual cycle not removed by the first criterion.

C. Dead-time-corrected decay curve fitting

The fitting of the decay-curve data was performed using a Levenberg-Marquardt χ^2 minimization algorithm [12] modified to incorporate dead-time-corrected Poisson-distributed data. Because of the failure of the Gaussian approximation in the limit of low numbers of counts per bin, it was necessary to modify the algorithm to incorporate Poisson distributed data using a χ^2 derived from a direct application of maximum likelihood to the Poisson probability distribution. The resulting

χ^2 can be written as follows [13]:

$$\chi^2 = 2\sum_{i=1}^{N} y_{\rm fit} - y_i + y_i \ln \frac{y_i}{y_{\rm fit}}, \quad (1)$$

where y_i is the dead-time-corrected number of counts in the ith bin, $y_{\rm fit}$ is the value of the fit function in that bin, and N is the total number of bins being considered. The above definition of χ^2 is independent of the variances σ_i^2 of the individual data points. This version of χ^2 will therefore not respond to increases in the variances that are associated with the dead-time correction. To take the increased variances into account one must include a bin-by-bin weighting factor, W_i, which can be written as the ratio of the effective variance for pure Poisson statistics, y_i, to the true variance σ_i^2 associated with the dead-time-corrected data [9] as follows:

$$W_i = \frac{y_i}{\sigma_i^2}. \quad (2)$$

The dead-time-corrected number of counts y_i and associated variances σ_i^2 are related to the measured number of counts n_i, the constant dead time per event τ, and the bin time t_b through [9] the following:

$$y_i = \frac{n_i}{1 - n_i\left(\frac{\tau}{t_b}\right)}, \quad (3)$$

$$\sigma_i^2 = \frac{n_i}{\left[1 - n_i\left(\frac{\tau}{t_b}\right)\right]^2}. \quad (4)$$

The appropriate χ^2 to be included in the the fitting routine in the case of dead-time-corrected Poisson distributed data is, therefore, as follows:

$$\chi^2 = 2\sum_{i=1}^{N} W_i \left(y_{\rm fit} - y_i + y_i \ln \frac{y_i}{y_{\rm fit}} \right). \quad (5)$$

A fitting program was developed that combined the χ^2 derived from Poisson statistics, the appropriate weighting factor to incorporate a dead-time correction, and the general Levenberg-Marquardt fit algorithm [12]. This method yields unbiased estimates of the fit parameters independent of the numbers of counts per bin and has been verified by detailed Monte Carlo simulations of dead-time-effected radioactive decay.

D. Half-life analysis and results

Following the preselection criteria, each cycle was dead-time corrected using the measured dead times (Sec. II A). The cycles from a given run were then summed and fit using the χ^2 minimization algorithm described above. In the case of two exponential decays (^{26}Na and ^{26m}Al) plus a constant background, the fit function can be expressed as follows:

$$y_{\rm fit}(t) = \int_{t_s}^{t_f} a_1 \exp\left(-\frac{\ln 2t}{a_2}\right) + a_3 \exp\left(-\frac{\ln 2t}{a_4}\right) + a_5\, dt, \quad (6)$$

where t_s and t_f are the starting and finishing times of the bin (i.e., $t_b = t_f - t_s$), respectively. The fit parameters are the constant background rate (a_5), the initial activities of the primary (a_1) and secondary (a_3) decays in counts per second, and their respective half-lives (a_2 and a_4). The half-life of ^{26m}Al was fixed at its central value $T_{1/2} = 6.3449 \pm 0.0019$ s [10] (i.e., $a_4 = 6.3449$ s) that reduced the fit function to four free parameters. Uncertainties in the ^{26m}Al half-life and the measured dead times are considered below.

A typical dead-time-corrected decay curve obtained from one of the MCSs with the resultant best fit curve overlayed for comparison is shown in Fig. 2. A plot of the half-lives obtained versus the run number is given in Fig. 3. The half-life of ^{26}Na, $T_{1/2} = 1.07128 \pm 0.00013$ s, is obtained from the weighted average of the 24 data sets presented in Fig. 3.

E. Systematic uncertainties

Several modifications to the input parameters of the fitting routine were made to explore stability and consistency of the above results. A summary of the modifications made and their effect on the deduced ^{26}Na half-life is given in Table I. The uncertainty associated with the ^{26m}Al half-life and the measured dead times were explored by fixing these parameters at the limits of their measured uncertainties. The resulting half-life obtained for ^{26}Na differed by less than 10^{-5} s because of the uncertainty in the ^{26m}Al half-life and by 5×10^{-5} s in the case of the dead-time uncertainties (see Table II).

Further consistency checks were made such as freeing the half-life of ^{26m}Al. Freeing an additional parameter in the fit function leads to an overall increase in the statistical uncertainty; however, as shown in Table I this causes no significant change to the resulting ^{26}Na half-life. Furthermore, a weighted average of the 24 deduced ^{26m}Al half-life values yielded $T_{1/2} = 6.342 \pm 0.066$ s and agrees with the high-precision value of $T_{1/2} = 6.3449 \pm 0.0019$ s [10]. Note that this measurement of the ^{26m}Al half-life to $\pm 1\%$ is achieved with a $\approx$0.3% contaminant activity.

A γ-ray singles spectrum was obtained at the time of this experiment with the 8π γ-ray spectrometer to determine if there were any other possible isobaric contamination of the beam. Although no contamination was observed, upper limits were determined from peak-area fits to the most intense γ rays, 829.4 and 82.5 keV for ^{26}Si and ^{26}Ne β decay, respectively [14], normalized to the intensity of the 1809-keV γ ray in ^{26}Mg. The areas of the resulting fits were consistent with zero; however, the upper limits were obtained by summing this with their respective 1σ uncertainties. These possible contaminations (relative to the 1809 keV) were 1.8×10^{-4} and 1.0×10^{-4} for ^{26}Si and ^{26}Ne, respectively, and were included by refitting the data using a fit function composed of four exponentials plus a constant background. The intensities of Si and Ne were fixed at their upper limits, whereas the half-lives were fixed at their known values of 2.234 s and 197 ms [14], respectively. These activities did not change the deduced half-life for ^{26}Na by more than 1 part per million (ppm).

As a final consistency check, channels were systematically removed from the beginning of the data set to investigate any possible rate-dependent effects. A plot of the deduced

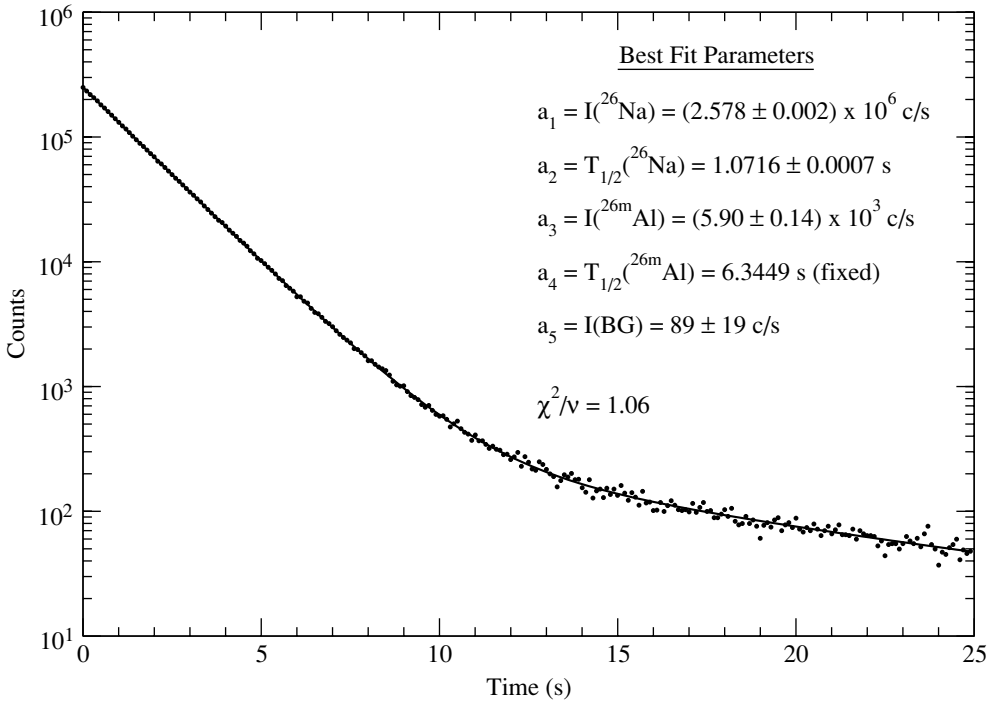

FIG. 2. Typical dead-time-corrected decay curve containing 156 cycles obtained from one MCS for a single run (run 10).

^{26}Na half-life versus the number of channels removed is given in Fig. 4. The uncertainties on the deduced half-life in this analysis systematically increase as a result of removing the channels with the highest statistics. The data are not randomly scattered about the mean because these are highly correlated rather than independent estimates of the half-life. Removing the channels with the highest statistics had no systematic effect in the determination of the half-life of ^{26}Na.

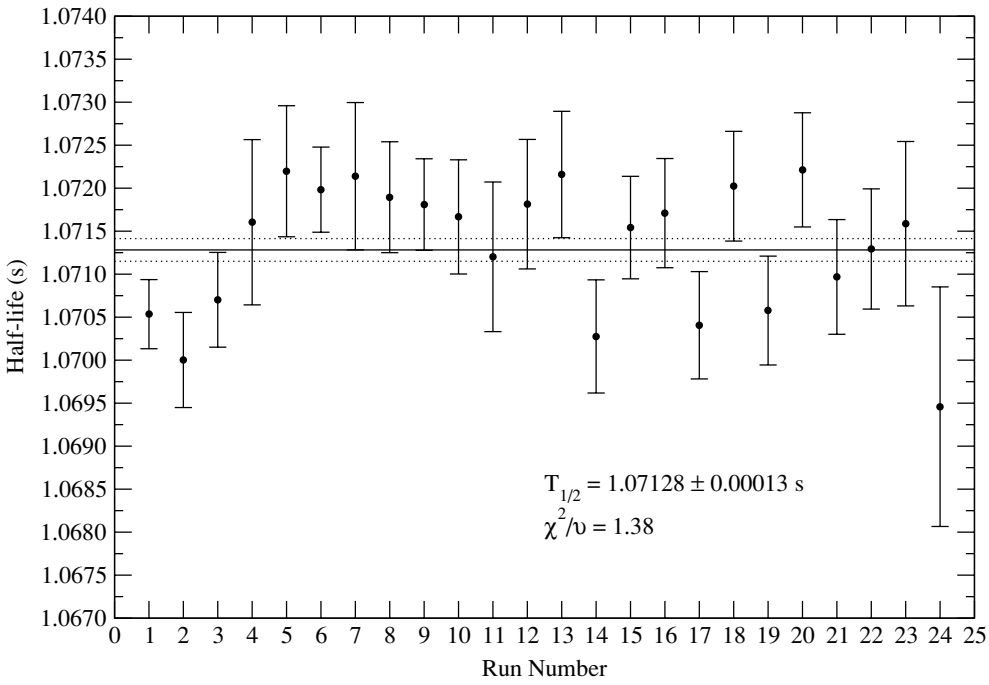

FIG. 3. Half-life versus run number obtained with the 4π continuous gas flow proportional counter and fast tape transport system. The solid line represents the deduced half-life (1.07128 s) obtained from a weighted average of these 24 data sets, whereas the dotted lines indicate the 1σ uncertainties ($\pm$0.00013 s).

TABLE I. Effect of input parameter adjustments on the deduced ^{26}Na half-life. The effect of the uncertainties of the input parameters such as dead times (τ) and the ^{26m}Al half-life were explored by altering these values within their 1σ limits.

Fit description	$T_{1/2}$(s)	$\sigma(T_{1/2})$(s)
Total data set	1.07128	0.00013
Fix $T^{Al}_{1/2} = 6.3430$ s	1.07128	0.00013
Fix $T^{Al}_{1/2} = 6.3468$ s	1.07129	0.00013
Free $T^{Al}_{1/2}$	1.07125	0.00018
$\tau_1 = 3.036\ \mu$s	1.07125	0.00013
$\tau_1 = 3.012\ \mu$s	1.07132	0.00013
$\tau_2 = 4.048\ \mu$s	1.07125	0.00013
$\tau_2 = 4.024\ \mu$s	1.07132	0.00013
^{26}Si [N(^{26}Si)/N(^{26}Na)] $= 1.8 \times 10^{-4}$	1.07128	0.00013
^{26}Ne [N(^{26}Ne)/N(^{26}Na)] $= 1.0 \times 10^{-4}$	1.07128	0.00013
^{26}Si and ^{26}Ne	1.07128	0.00013

To investigate potential systematic contributions from the electronics, the half-lives deduced on a run-by-run basis (Fig. 3) were combined and averaged according to common electronic settings. All such combinations considered are plotted in Fig. 5. Overlaid for comparison is the overall deduced half-life $T_{1/2} = 1.07128 \pm 0.00013$ s, which acts as a means to highlight any inconsistencies.

The two MCSs yielded statistically identical results and hence the average of the half-lives deduced from both of these scalars was used to determine the run by run half-lives presented in Fig. 3. Treating the 24 runs presented in Fig. 3 as 24 independent measurements of the half-life, we obtain a reduced χ^2 of 1.38. To estimate a systematic uncertainty, we adopt the particle data group method [15], which increases the experimental error by the square root of the reduced χ^2 if the reduced χ^2 is greater than unity. For the 24 runs presented in Fig. 3 we therefore increase our statistical uncertainty by 1.17 from 0.00013 s to 0.00015 s. The systematic uncertainty is then chosen so that when added in quadrature with the statistical uncertainty (0.00013 s) yields the estimate of the total uncertainty (0.00015 s). For this comparison we would assign a systematic uncertainty of ± 0.00008 s. The assignment of this systematic uncertainty is based solely on the statistical fluctuations observed in Fig. 3. Inspection of Fig. 5 does, however, indicate that there are three possible sources of systematic uncertainty resulting from the electronic settings employed.

TABLE II. Sources of systematic uncertainty and their contributions to the overall estimate of ± 0.00021 s. The contributions from the dead times, ^{26m}Al half-life, and contaminants were deduced by altering these parameters between their 1σ limits and observing their effects on the half-life of ^{26}Na (from Table I).

Source	Contribution (s)
Electronics (bin-time settings)	0.00020
Uncertainty in dead times	0.00005
Uncertainty in ^{26m}Al half-life	$<10^{-5}$
Contamination from ^{26}Si and ^{26}Ne	$<10^{-6}$
Total estimated systematic uncertainty (added in quadrature)	0.00021

The 24 runs collected in this work were obtained using six different voltage settings. Treating these six settings as independent measurements with a mean of 1.07128 ± 0.00013 s, the reduced χ^2 is 2.95. Using the particle data groups method described above, the estimate for the systematic uncertainty is ± 0.00018 s. For the three discriminator/timing filter amplifier (TFA) settings, the reduced χ^2 is 2.06, which would correspond to a systematic uncertainty estimate of ± 0.00014 s. A final comparison can be made with the three different bin times that yield a reduced χ^2 of 3.31, corresponding to a systematic uncertainty of ± 0.00020 s. As a conservative estimate we choose the comparison that yields that largest value and assign ± 0.00020 s as a systematic uncertainty that is almost entirely due to the value obtained with a bin-time setting of 0.2 s.

The half-life of ^{26}Na obtained at a bin time of 0.2 s was $T_{1/2} = 1.07000 \pm 0.00055$ s, which differs from the mean value of the half-life, $T_{1/2} = 1.07128 \pm 0.00013$ s, by 2.3σ. It should, however, be emphasized that this result is composed of only a single run (run 2). Because only one run was used it is difficult to determine whether this particular setting was faulty or whether the observed result is nothing more than a statistical fluctuation at the 2.3σ level. This run has been carefully scrutinized and we have found no reason to omit this data point in the final determination of the half-life of ^{26}Na.

A summary of the possible sources of systematic uncertainty and their contribution to the overall estimated systematic uncertainty of ± 0.00021 s is given in Table II. The overall half-life of ^{26}Na is therefore $T_{1/2} = 1.07128 \pm 0.00013 \pm 0.00021$ s. The first uncertainty is statistical, whereas the second is an estimated systematic uncertainty resulting primarily from the small discrepancy in the half-life obtained at a bin time of 0.2 s. A weighted average of all previous measurements of the ^{26}Na half-life: $T_{1/2} = 1.074(6)$ s [16], 1.087(12) s [17], 1.05(2) s [18], 1.070(30) s [19], 1.03(6) s [20], and 1.04(3) s [21] yields $T_{1/2} = 1.073 \pm 0.005$ s. The weighted average of the literature values agree with the result presented in this work, but is more than 20 times less precise.

III. β-BRANCHING RATIOS

A. Experimental setup

The 8π γ-ray spectrometer consists of 20 Compton-suppressed HPGe γ-ray detectors arranged in a spherically symmetric array surrounding the implantation site of a new low-energy beam line at ISAC. The detectors are each equipped with tungsten collimators that prevent γ rays from directly striking the Compton suppression shields and are covered with approximately 2-cm-thick plastic (Delrin) that acts to minimize bremsstrahlung production from high-energy β particles (up to $\approx$7.5 MeV for ^{26}Na β decay).

A continuous beam of ^{26}Na for this experiment was produced with the ISAC surface ion source coupled to a Ta production target. The beam was implanted on a thin aluminum disk at the center of the 8π, and γ rays following the β^- decay

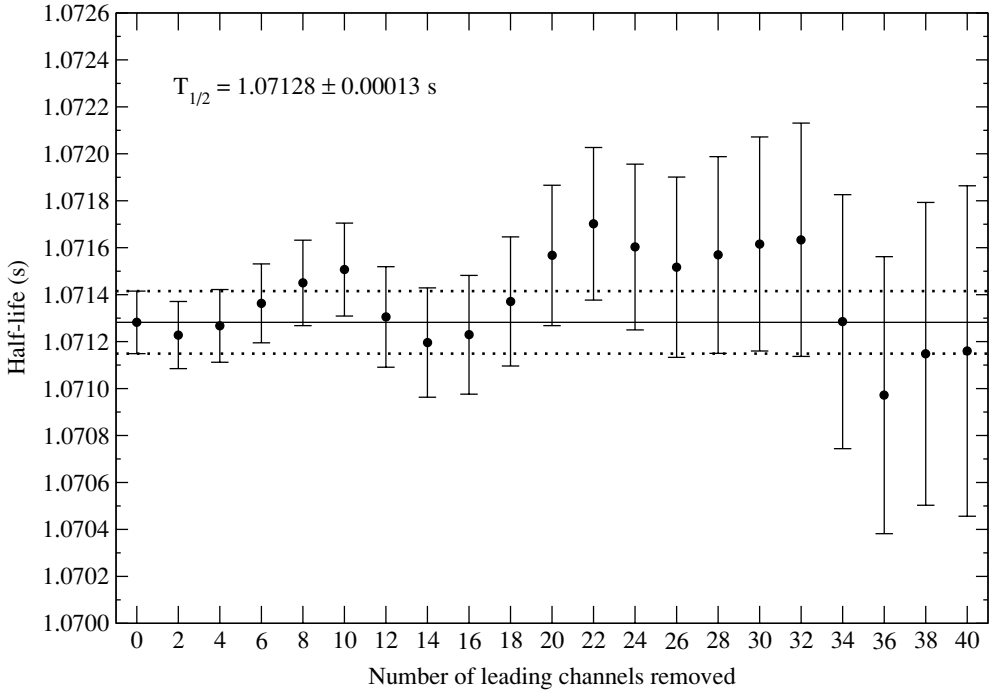

FIG. 4. Effect of removing leading channels on the deduced ^{26}Na half-life. Each data point presented here is obtained by removing the two leading channels from the previous data point. The half-life obtained in this work is overlayed for comparison as one cannot perform a linear regression to these highly correlated data.

of ^{26}Na to ^{26}Mg were observed. Standard calibration sources of ^{152}Eu and ^{56}Co were used to calibrate the γ-ray energies and relative efficiencies up to 3.4 MeV. At higher energies, our energy calibration was obtained by an extrapolation of the ^{152}Eu and ^{56}Co data, including the 6128.6-keV γ ray [22] from ^{16}N β decay (a common background line observed

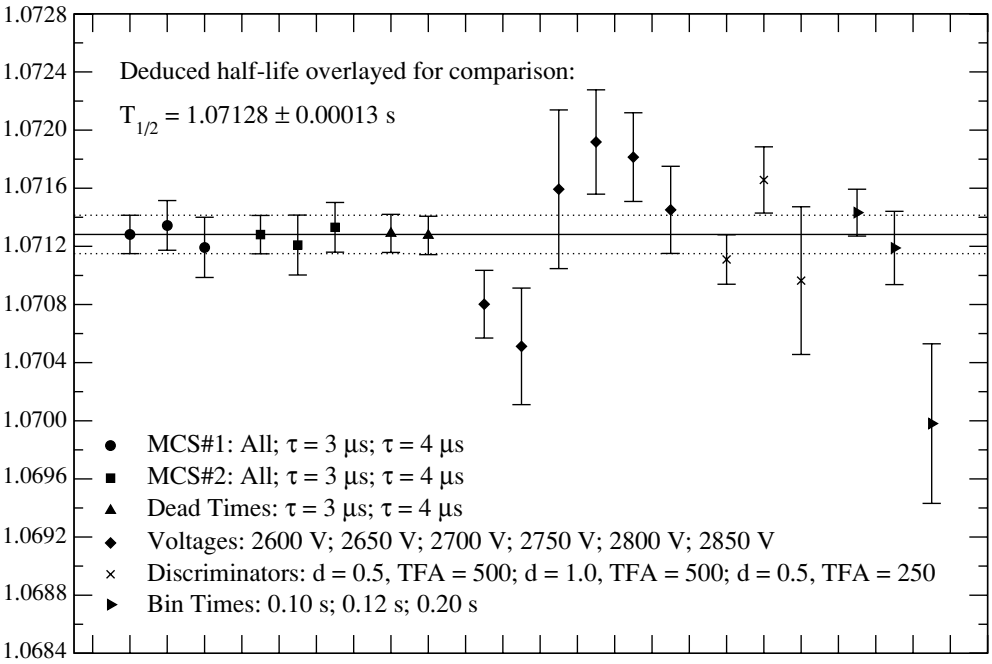

FIG. 5. Half-life measurements of ^{26}Na sorted by adjustable electronic setting. Each data point corresponds to a different grouping as indicated in the legend. As an example, the first three data points correspond to the half-life obtained with the first MCS, the half-life obtained with the first MCS with a fixed dead time per event of 3.024 ± 0.012 μs, and the half-life obtained with the first MCS with a fixed dead time per event of 4.036 ± 0.012 μs, respectively.

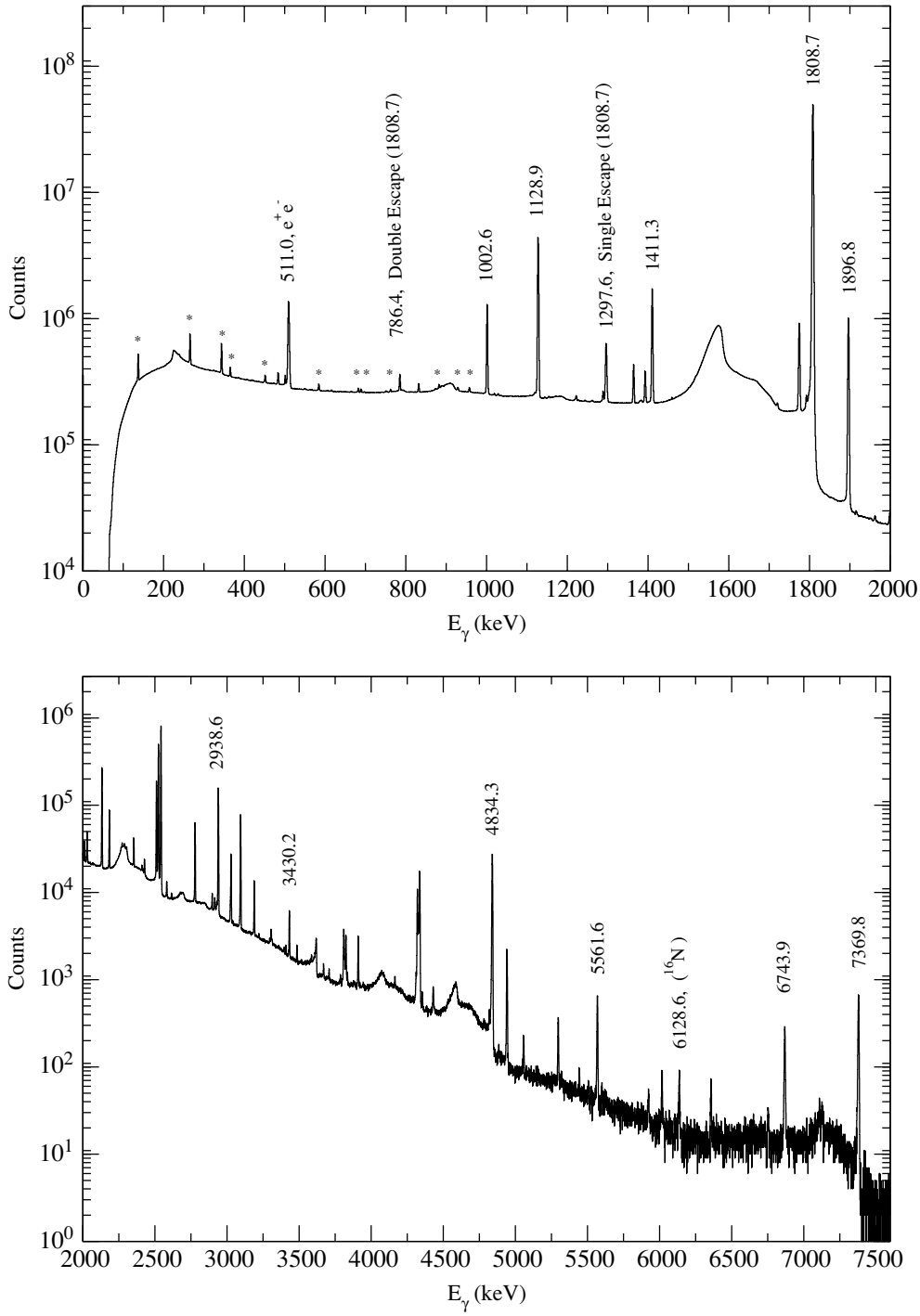

FIG. 6. γ-ray singles spectrum for the entire data set obtained from approximately 12 hours of beam at $\sim 10^5$ s^{-1}. A total of $(1.5419 \pm 0.0002) \times 10^8$ counts were observed in the 1808.7-keV photopeak. Several γ rays from the β decay of ^{156}Tm (indicated by an asterisk) are visible at low energies.

in radioactive beam facilities), as well as the 4834.3- and 7369.8-keV γ rays from ^{26}Mg [23]. Relative efficiencies up to 7.5 MeV were calculated from a GEANT4 simulation [24] normalized to the 1808.7-keV transition in ^{26}Mg. This simulation agrees with the highest experimental energy value from ^{56}Co at 3451 keV to 0.2% and yields an uncertainty of $\pm 10\%$ on the relative efficiency at the highest-energy γ ray in ^{26}Mg (7369.8 keV).

A γ-ray singles spectrum containing the entire data set ($\approx$12 hr live time) is shown in Fig. 6. A total of 1.54×10^8 counts were observed in the 1809-keV photopeak. Several of the low-energy peaks in Fig. 6 are γ rays that follow the electron-capture decays of ^{156}Tm and ^{156}Er. One possible source of these heavy ions (with $A = 26 \times 6 = 156$) in a 6^+ charge state is multiple Auger electron emission following the electron-capture decay of ^{156}Yb produced in the target.

TABLE III. ^{26}Mg energy level and decay data. A total of 84 γ rays have been identified following the β^- decay of ^{26}Na. Level energies were obtained from the γ-ray energies and include the nuclear recoil correction factor. Intensities are relative to 100% for the 1808.71-keV transition. Spin and parity assignments are those of Ref. [22].

E_x (keV)	β-Branch (%)	${}_iI_n^\pi$	${}_fI_n^\pi$	E_γ (keV)	I (%)
1808.78(20)	87.80(7)	2_1^+	0_0^+	1808.71(20)	100
2937.98(21)	0.05(4)	2_2^+	2_1^+	1128.89(13)	5.927(29)
			0_0^+	2938.6(4)	0.570(19)
3940.80(25)	1.31(4)	3_1^+	2_2^+	1002.61(12)	1.282(8)
			2_1^+	2132.91(25)	0.637(7)
4318.89(27)	0.493(11)	4_1^+	2_2^+	1380.88(18)	0.0095(6)
			2_1^+	2510.52(32)	0.514(11)
4332.02(25)	1.648(31)	2_3^+	2_2^+	1393.83(15)	0.2878(11)
			2_1^+	2524.10(32)	1.430(31)
			0_0^+	4332.1(9)	0.115(8)
4349.80(25)	3.17(7)	3_2^+	3_1^+	409.22(20)[a]	0.0010(6)
			2_2^+	1411.32(16)	2.466(7)
			2_1^+	2541.57(32)	2.39(5)
4835.05(24)	2.378(19)	2_4^+	3_2^+	485.05(9)	0.0575(9)
			2_3^+	502.73(9)	0.0550(8)
			3_1^+	892.85(19)	0.0053(7)
			2_2^+	1896.78(22)	2.074(7)
			2_1^+	3026.6(5)	0.0868(32)
			0_0^+	4834.3(10)	0.225(17)
4901.36(25)	0.246(11)	4_2^+	3_2^+	551.28(13)	0.0046(4)
			2_3^+	569.67(25)	0.00186(34)
			4_1^+	582.46(21)	0.0025(5)
			3_1^+	958.81(12)	0.0110(13)
			2_2^+	1962.99(24)	0.0054(4)
			2_1^+	3092.8(4)	0.285(11)
5291.40(30)	0.0129(18)	2_5^+	2_4^+	456.0(4)	0.0012(4)
			3_1^+	1349.4(4)	0.0026(6)
			2_2^+	2353.74(29)	0.0626(12)
			2_1^+	3482.0(7)	0.00246(25)
			0_0^+	5290.82(30)[a]	0.00234(23)
5475.73(34)	0.0027(12)	4_3^+	2_4^+	640.53(31)	0.0014(4)
			4_1^+	1155.85(17)	0.0074(9)
			2_1^+	3667.5(6)	0.00195(18)
5716.45(26)	0.94(4)	4_4^+	4_3^+	240.12(11)	0.0080(6)
			2_5^+	424.30(31)	0.00136(31)
			3_2^+	1365.21(15)	0.3517(15)
			2_3^+	1384.70(16)	0.0163(6)
			3_1^+	1775.08(20)[a]	0.37(4)
			2_2^+	2777.7(4)	0.190(5)
			2_1^+	3906.8(7)	0.0124(8)
6125.55(26)	1.72(4)	3_3^+	4_4^+	409.22(20)[a]	0.0012(6)
			2_5^+	833.26(10)	0.0501(8)
			4_2^+	1223.35(15)	0.0325(11)
			2_4^+	1289.88(14)	0.0890(12)
			3_2^+	1775.08(20)[a]	1.20(4)
			2_3^+	1792.90(20)	0.0795(12)
			3_1^+	2184.11(26)	0.1807(22)

TABLE III. (*Continued.*)

E_x (keV)	β-Branch (%)	${}_iI_n^\pi$	${}_fI_n^\pi$	E_γ (keV)	I (%)
			2_2^+	3187.3(5)	0.0426(18)
			2_1^+	4316.3(8)	0.072(5)
6623.37(30)	0.0607(12)	4_5^+	4_2^+	1721.39(20)	0.0290(10)
			3_2^+	2272.73(28)	0.0127(5)
			2_3^+	2290.16(30)	0.0076(4)
			4_1^+	2304.20(29)	0.0109(5)
			2_1^+	4813.7(10)	0.00110(14)
6744.6(5)	0.0414(20)	2_6^+	2_5^+	1453.16(17)	0.0044(6)
			2_2^+	3806.7(6)	0.0186(11)
			2_1^+	4936.1(11)	0.0184(14)
			0_0^+	6743.9(21)	0.00035(8)
7098.8(8)	0.0028(9)	2_7^+	2_2^+	4160.6(8)	0.00175(21)
			2_1^+	5289.4(8)[a]	0.00066(14)
			0_0^+	7099.0(24)	0.00046(7)
7246.69(30)	0.0507(16)	3_4^+	3_3^+	1120.74(24)	0.0074(11)
			2_5^+	1953.6(7)	0.0012(5)
			2_4^+	2411.47(30)	0.0113(4)
			3_2^+	2896.4(4)	0.0110(5)
			2_3^+	2913.7(4)	0.0067(4)
			4_1^+	2927.2(5)	0.0025(3)
			3_1^+	3304.6(5)	0.0058(3)
			2_2^+	4308.1(8)	0.0048(3)
			2_1^+	5436.1(13)	0.00041(8)
7372.1(4)	0.0608(22)	2_8^+	3_3^+	1245.68(24)	0.0074(9)
			2_5^+	2080.0(6)	0.00100(29)
			3_2^+	3022.0(4)	0.0124(5)
			2_3^+	3039.1(5)	0.00124(18)
			3_1^+	3430.2(5)	0.0197(9)
			2_1^+	5561.6(14)	0.0065(6)
			0_0^+	7369.8(25)	0.0131(15)
7726.2(5)	0.0035(7)	3_5^+	4_1^+	3406.9(5)	0.00209(17)
			3_1^+	3783.7(7)	0.00104(13)
			2_1^+	5915.5(16)	0.00042(8)
7774.0(6)	0.0024(7)	4_6^+	4_1^+	3454.7(9)	0.00034(12)
			3_1^+	3831.7(7)	0.00207(19)
7818.2(8)	0.0023(10)	$(2,3)^+$	2_3^+	3485.0(7)	0.00137(20)
			2_1^+	6008.7(16)	0.00092(12)

[a]Doublet.

From the singles and coincidence spectra collected in this experiment, a total of 84 γ-ray transitions from 20 excited states were observed in the β decay of ^{26}Na. This is an increase over previous work in which 20 γ rays from 11 populated levels were identified [17,18]. A summary of observed γ-ray energies and intensities relative to the 1809-keV transition is presented in Table III. Relative γ-ray intensities have been corrected for coincident summing effects both into and out of the peak. The latter correction was generally the dominant, ranging from approximately 0.2 to 3%. Level energies were calculated from the measured γ-ray energies and include a correction for the nuclear recoil. Significant figures and rounding procedures for this work were adopted from the method of the particle data group [15].

Three γ-ray energies appear in Table III as doublets because differences between energy levels in distinct locations of the level scheme yield the same γ-ray energy within error. The intensities and their respective uncertainties for the 409.2- and 1775.1-keV γ rays were estimated from the coincidence spectrum, with the relatively large uncertainties reflecting the statistics obtained in the γ-γ coincidence data. The $\sim$5290-keV doublet could not be resolved from the coincidence spectrum; however, the existence of both of these transitions has been previously established [25]. Relative

TABLE IV. β-Branching ratios deduced from ^{26}Na β^- decay to excited states in ^{26}Mg. Branching ratios previously unknown are indicated by a dash.

Energy level (keV)	β-Branch (%) present work	β-Branch (%) Ref. [17]	β-Branch (%) Ref. [18]
1809	87.80(7)	87.9(4)	87.9(2.0)
2938	0.05(4)	<0.8	(0.1)
3941	1.31(4)	1.3(4)	1.7(2)
4319	0.493(11)	0.54(14)	0.5(1)
4332	1.648(31)	1.54(14)	2.0(2)
4350	3.17(7)	5.6(4)	2.7(3)
4835	2.378(19)	2.9(2)	2.5(2)
4901	0.246(11)	<0.6	0.3(1)
5291	0.0129(19)	<0.3	—
5476	0.0027(12)	—	<0.04
5716	0.94(4)	—	0.7(1)
6126	1.72(4)	—	1.7(2)
6623	0.0607(12)	—	—
6745	0.0414(20)	—	—
7099	0.0028(9)	—	—
7247	0.0507(16)	—	—
7372	0.0608(22)	—	—
7726	0.0035(7)	—	—
7774	0.0024(7)	—	—
7818	0.0023(10)	—	—

intensities for this doublet were deduced from fitting two distributions to the observed peak with the centroids fixed at 5289.4 and 5290.8 keV, the energies deduced from the differences in energy levels 7098.8(8)–1808.78(20) keV and 5291.40(30)–0.0 keV (including the nuclear recoil correction factor), respectively.

B. β-Branching ratio analysis and results

In the case of ^{26}Na β decay we can neglect the second forbidden β-decay branch to the ^{26}Mg ground state (a small correction is made for such a branch below). The β-branching ratio to the ith excited energy level can therefore be determined from the *relative* γ-ray intensities,

$$B_i = \frac{I_{i,\mathrm{out}} - I_{i,\mathrm{in}}}{I_{\mathrm{tot}}}, \tag{7}$$

where $I_{i,\mathrm{out}}(I_{i,\mathrm{in}})$ represents the total γ-ray intensity (corrected for relative detection efficiencies) observed decaying out of (into) the ith level. The total intensity, I_{tot}, is equal to the total intensity of γ rays feeding the 0^+ ground state.

The β-branching ratios deduced from this experiment are given in Table IV and are compared with previous determinations. Results from this work are generally an order of magnitude more precise. Energy levels given in Table IV and adopted as labels for the rest of this work were obtained from the calculated levels presented in Table III rounded to the nearest integer.

C. β-Branching-ratio uncertainties

In addition to the uncertainties in the relative γ-ray intensities themselves, small corrections to Eq. (7), originating from several sources, must be considered. It should be emphasized that all of the effects discussed here were used only as a means to increase the experimental uncertainties of the three quantities I_{tot}, $I_{i,\mathrm{in}}$, and $I_{i,\mathrm{out}}$ used to calculate the β-branching ratios [Eq. (7)]. They were not used to alter the central values given in Table IV.

1. Unobserved β decay to the ground state

There is in principle a β branch to the ground state in which case no γ rays would be observed. This decay, however, is a second forbidden transition and is expected to be suppressed by many orders of magnitude. We estimated a contribution of 0.01 ppm, which was added directly to the uncertainty in the ground-state intensity, I_{tot}.

2. Unobserved ground-state γ-ray transitions

There were excited levels for which a decay to the ground state was not observed when in principle, it could have occurred. Considering only $E1$, $M1$, and $E2$ transitions, the energy levels at excitation energies 7818 and 7247 keV had no observed decay to the ground state but could have decayed directly via $E2$ transitions. Upper limits on these transitions were determined from the γ-ray singles spectrum and the uncertainty on the total ground-state intensity I_{tot} was inflated by 0.03 ppm to account for them.

3. Unobserved γ-ray transitions between levels

There are in principle γ-ray transitions between known energy levels that were too weak to be observed. Upper limits for the intensities of these transitions were estimated from the γ-ray singles spectrum for all $E1$, $M1$, and $E2$ transitions that were not observed. Error estimates were obtained for both the $I_{i,\mathrm{out}}$ and the $I_{i,\mathrm{in}}$ transitions by summing the 1σ limits for the unobserved γ rays in quadrature with the existing uncertainties in the numbers of counts on a level-by-level basis. This effect varies in size from several percent as in the case of the 7818-keV level where several potential γ rays from this level were unobserved, to negligibly small as in the case of the 1809-keV level, where all possible transitions were already observed.

4. β decay to highly excited states in ^{26}Mg

The final contribution to the systematic uncertainty considered involves unobserved states at high energies. There are 11 possible 2^+, 3^+, or 4^+ levels in ^{26}Mg between 7818 keV (the highest observed level) and 9352 keV (the Q value for the β decay) [22]. Some of these high-energy levels could be fed by the β decay and then supply a small γ ray feeding to the levels that were observed in this work. Although the known γ rays from these high-energy levels had measured intensities consistent with zero, this correction was estimated by taking the sum of the 1σ limits of these intensities. This sum was then taken as an upper limit on the total intensity with which this high-energy group of states is fed by the β decay. The total intensity was then distributed to the uncertainties of the feeding ($I_{i,\mathrm{in}}$) of all of the lower energy levels (except the ground state)

TABLE V. Comparison of the $\log ft$ values obtained in the present work with previous determinations. $\log ft$ values previously unknown are indicated by a dash.

Energy level (keV)	$\log ft$ present work	$\log ft$ Ref. [17]	$\log ft$ Ref. [18]
1809	4.7181(17)	4.72(2)	4.72(2)
2938	7.63(32)	>6.5	(7.3)
3941	5.875(14)	5.86(11)	5.76(10)
4319	6.154(10)	6.11(10)	6.15(10)
4332	5.625(9)	5.65(4)	5.54(10)
4350	5.334(9)	5.08(3)	5.40(8)
4835	5.257(4)	5.16(3)	5.23(7)
4901	6.212(19)	>5.8	6.12(15)
5291	7.31(6)	>5.9	—
5476	7.90(20)	—	—
5716	5.234(19)	—	5.36(10)
6126	4.741(11)	—	4.75(10)
6623	5.873(10)	—	—
6745	5.954(21)	—	—
7099	6.85(15)	—	—
7247	5.466(15)	—	—
7372	5.274(17)	—	—
7726	6.15(9)	—	—
7774	6.27(12)	—	—
7818	6.24(19)	—	—

weighted by E_γ^3 (the Weisskopf estimate for dipole transitions). A total estimate of this feeding was of the order 1 ppm. As 2^+ states in these unobserved high-energy levels could also have $E2$ decay branches directly to the ground state, a 1-ppm inflation to the uncertainty of $I_{\rm tot}$ was also applied.

The corrections discussed above were applied in the calculation of the uncertainties on the β-branching ratios presented in Table IV.

IV. ft VALUES

A. Experimental determination

Calculation of experimental ft values requires measurements of three fundamental quantities: (a) the half-life, (b) the β-branching ratios, and (c) the Q value of the decay. With (a) and (b) established in Secs. II and III of this work, respectively, the ft values were then computed using the known Q value to the ground state, $Q_o = 9352 \pm 6$ keV [6]. The half-life and β-branching ratios deduced in the present work yield $\log ft$ values in agreement with, but approximately an order of magnitude more precise than, previous determinations (Table V). Further improvements in the precision of the $\log ft$ values are generally limited by the uncertainties in the β-branching ratios.

B. Comparison to theory

The $\log ft$ values presented in the previous section were determined from independent experimental measurements of the half-life and β-branching ratios combined with the known Q value. Theoretical calculations of the $\log ft$ values were performed using the OXBASH code [26]. Wave functions for ^{26}Mg were deduced using a full *sd*-shell model calculation with

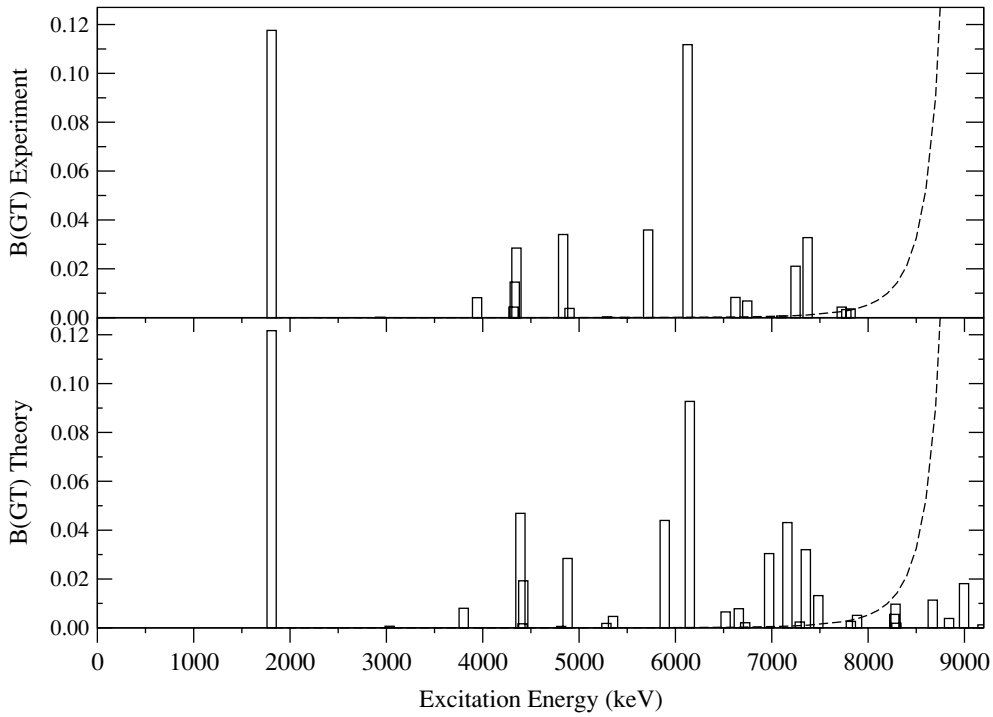

FIG. 7. Comparison of B(GT) values from experiment (top panel) to a full *sd*-shell-model calculation (bottom panel) for all $I^\pi = 2^+, 3^+, 4^+$ states in ^{26}Mg. The experimental sensitivity curve (indicated by the dashed line) is the boundary below which the β-branching ratios are expected to be too weak ($<2 \times 10^{-5}$) to be measured experimentally.

TABLE VI. Comparison of the experimental and theoretical $\log ft$ values obtained in this work.

Experiment			Theory		
E_x (keV)	I_n^π	$\log ft$	E_x (keV)	I_n^π	$\log ft$
1809	2_1^+	4.7181(17)	1809	2_1^+	4.7033
2938	2_2^+	7.63(32)	3034	2_2^+	6.97
3941	3_1^+	5.875(14)	3802	3_1^+	5.884
4319	4_1^+	6.155(10)	4413	4_1^+	6.568
4332	2_3^+	5.625(9)	4421	2_3^+	5.504
4350	3_2^+	5.334(9)	4391	3_2^+	5.118
4835	2_4^+	5.257(4)	4881	2_4^+	5.335
4901	4_2^+	6.212(19)	4813	4_2^+	7.028
5291	2_5^+	7.31(6)	5284	2_5^+	6.53
5476	4_3^+	7.90(20)	5353	4_3^+	6.12
5716	4_4^+	5.234(19)	5889	4_4^+	5.145
6126	3_3^+	4.741(11)	6149	3_3^+	4.821
6623	4_5^+	5.873(10)	6658	4_5^+	5.894
6745	2_6^+	5.954(21)	6521	2_6^+	5.973
7099	2_7^+	6.85(15)	6724	2_7^+	6.46
7247	3_4^+	5.466(15)	7162	3_4^+	5.154
7372	2_8^+	5.274(17)	6973	2_8^+	5.305
7726	3_5^+	6.15(9)	7483	3_5^+	5.668
7774	4_6^+	6.27(12)	7291	4_6^+	6.41
7818	$(2,3)^+$	6.24(19)			

the USD interaction [27]. The formalism for calculation of the Gamow-Teller single-particle matrix elements is described in detail in Ref. [28].

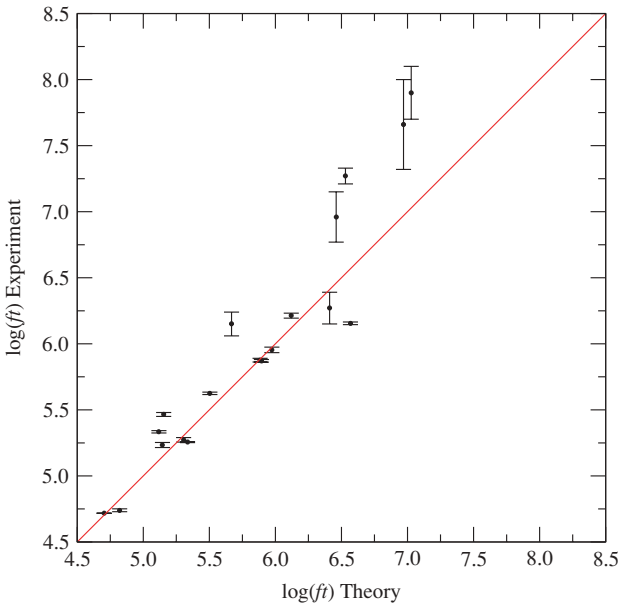

FIG. 8. (Color online) Comparison of the experimental $\log ft$ values versus the theoretical $\log ft$ values. Perfect agreement between experiment and theory in this figure would correspond to the $y = x$ diagonal.

A plot of the theoretical Gamow-Teller strengths is given in Fig. 7 for the first 10 theoretical states for each of $I^\pi = 2^+$, 3^+, and 4^+. Theoretical excitation energy values have been normalized at the 1809-keV energy level. The experimental B(GT) values presented in Fig. 7 were calculated from the ft values through the expression

$$B(GT) = \frac{2\mathcal{F}t}{ft}, \tag{8}$$

where $\mathcal{F}t = 3072.2 \pm 0.8$ s [2] is the average corrected ft value from the superallowed Fermi β decays. Also plotted in Fig. 7 is an experimental sensitivity curve (indicated by the dashed line) which is the boundary below which the β-branching ratios are expected to be too weak ($<2 \times 10^{-5}$) to be measured experimentally. This curve was obtained by fixing the β-branching ratio in Eq. (8) at 2×10^{-5}, just below the weakest experimental β branch measured.

Comparison of experimental and theoretical $\log ft$ values obtained for ^{26}Na are given in Table VI. In general there is excellent agreement for level energies up to and including the 7774-keV state with a clear state-by-state correspondence. The one exception is the 4_2^+ and 4_3^+ theoretical states, which, based on a comparison of B(GT) values, appear to have a stronger overlap of wave functions with the experimental 4_3^+ and 4_2^+ levels, respectively. A comparison with theory for the experimental 7818-keV level is not made because of uncertainties in the experimental spin and parity assignments. Another comparison between experiment and theory can be made by plotting the data in a $\log ft$ plane as shown in

Fig. 8, which plots the experimental $\log ft$ values with their uncertainty on the y axis versus the corresponding theoretical $\log ft$ values on the x axis. Perfect agreement between experiment and theory would correspond to the 1:1 diagonal as indicated. Although experimental and theoretical $\log ft$ values between 4.5 and 6.0 demonstrate excellent agreement, a clear systematic trend is evident for the $\log ft$ values greater than 6.5 in which theory tends to overestimate the strengths of these weak transitions.

V. CONCLUSION

From the γ-ray singles and coincidence spectra obtained with the 8π spectrometer, a total of 84 γ rays emitted from 20 excited states in ^{26}Mg have been observed. The β-branching ratios were determined for each of the 20 excited states and were found to generally agree with the previous measurements (where known), although they are roughly an order of magnitude more precise.

Combining the half-life of ^{26}Na deduced from the β-counting experiment, $T_{1/2} = 1.07128 \pm 0.00013 \pm 0.00021$ s, with the β-branching ratios and the known Q value, the $\log ft$ values for ^{26}Na β decay were determined. The $\log ft$ values deduced in this work were found to agree with previous determinations but, again, are nearly an order of magnitude more precise. Comparison of the experimental $\log ft$ values with the corresponding theoretical values resulting from a full *sd*-shell-model calculation yielded excellent agreement with a clear state-by-state correspondence for the first 19 excited states in ^{26}Mg.

ACKNOWLEDGMENTS

The authors thank B.G. Nickel for enlightening discussions and the staff of ISAC for delivery of the high-quality ^{26}Na beams. This work was partially supported by the Natural Sciences and Engineering Research Council of Canada, the Government of Ontario through a Premier's Research Excellence Award, the National Research Council of Canada, the Research Corporation through a Research Innovation Award, the Robert A. Welch Foundation, and the U.S. Department of Energy through contract DE-FG03-93ER40773.

[1] P. G. Bricault, M. Dombsky, P. W. Schmor, and G. Stanford, Nucl. Instrum. Methods Phys. Res. B **126**, 231 (1997).
[2] I. S. Towner and J. C. Hardy, Phys. Rev. C. **66**, 035501 (2002).
[3] C. E. Svensson *et al*., Nucl. Instrum. Methods Phys. Res. B **204**, 660 (2003).
[4] M. Dombsky *et al*., Rev. Sci. Instrum. **69**, 1170 (1998).
[5] E. Hagberg *et al*., Nucl. Phys. **A571**, 555 (1994).
[6] D. Lunney *et al*., Phys. Rev. C **64**, 054311 (2001).
[7] G. Audi, A. H. Wapstra, and C. Thibault, Nucl. Phys. **A729**, 337 (2003).
[8] V. T. Koslowsky *et al*., Nucl. Phys. **A405**, 29 (1983).
[9] V. T. Koslowsky *et al*., Nucl. Instrum. Methods Phys. Res. A **401**, 289 (1997).
[10] I. S Towner and J. C. Hardy, in *Physics beyond the Standard Model: Proceedings of the Fifth International WEIN Symposium*, edited by P. Herczeg *et al*. (World Scientific, Singapore, 1999), Vol. 338.
[11] A. P. Baerg, Metrologia **1**, No. 3, 131 (1965).
[12] W. H. Press *et al*., *Numerical Recipes in C*, 2nd ed. (Cambridge University Press, 1992).
[13] S. Baker and R. D. Cousins, Nucl. Instrum. Methods Phys. Res. **221**, 437 (1984).
[14] R. B. Firestone *et al*., *Table of Isotopes*, 8th ed. (Wiley, New York, 1996).
[15] S. Eidelman *et al*., Phys. Lett. **B592**, 1 (2004).
[16] O. Tengblad *et al*., Z. Phys. A **342**, 303 (1992).
[17] D. E. Alburger, D. R. Goosman, and C. N. Davids, Phys. Rev. C **8**, 1011 (1973).
[18] G. Klotz, J. P. Gonidec, P. Baumann, and G. Walter, Nucl. Phys. **A205**, 90 (1973).
[19] R. Klapisch, C. Thibault, A. M. Poskanzer, R. Prieels, C. Rigaud, and E. Roeckl, Phys. Rev. Lett. **29**, 1254 (1972).
[20] E. L. Robinson, B. T. Lucas, and O. E. Johnson, Phys. Rev. **122**, 202 (1961).
[21] M. J. Nurmia and R. W. Fink, Nucl. Phys. **8**, 139 (1958).
[22] P. M. Endt, Nucl. Phys. **A633**, 1 (1998).
[23] T. A. Walkiewicz, S. Raman, E. T. Jurney, J. W. Starner, and J. E. Lynn, Phys. Rev. C **45**, 1597 (1992).
[24] S. Agostinelli *et al*., Nucl. Instrum. Methods Phys. Res. A **506**, 250 (2003).
[25] P. M. Endt, Nucl. Phys. **A521**, 1 (1990).
[26] B. A. Brown, A. Etchegoyen, and W. D. M. Rae, Michigan State University Cyclotron Laboratory Report No. 524, 1985.
[27] B. H. Wildenthal, Prog. Part. Nucl. Phys. **11**, 5 (1984).
[28] B. A. Brown and B. H. Wildenthal, At. Data Nucl. Data Tables **33**, 347 (1985).